INTERFACE

royalsocietypublishing.org/journal/rsif

Research

Cite this article: Fadai NT, Baker RE, Simpson MJ. 2019 Accurate and efficient discretizations for stochastic models providing near agent-based spatial resolution at low computational cost. *J. R. Soc. Interface* **16**: 20190421. http://dx.doi.org/10.1098/rsif.2019.0421

Received: 17 June 2019
Accepted: 1 October 2019

Subject Category:
Life Sciences–Mathematics interface

Subject Areas:
biomathematics, computational biology

Keywords:
compartment-based model, lattice-based model, proliferation assay, scratch assay, crowding effects, volume exclusion

Author for correspondence:
Nabil T. Fadai
e-mail: nabil.fadai@qut.edu.au

Electronic supplementary material is available online at https://doi.org/10.6084/m9.figshare.c.4695536.

THE ROYAL SOCIETY PUBLISHING

Accurate and efficient discretizations for stochastic models providing near agent-based spatial resolution at low computational cost

Nabil T. Fadai[1], Ruth E. Baker[2] and Matthew J. Simpson[1]

[1]School of Mathematical Sciences, Queensland University of Technology, Brisbane, Queensland 4001, Australia
[2]Mathematical Institute, University of Oxford, Oxford OX2 6GG, UK

NTF, 0000-0001-7717-5421; REB, 0000-0002-6304-9333; MJS, 0000-0001-6254-313X

Understanding how cells proliferate, migrate and die in various environments is essential in determining how organisms develop and repair themselves. Continuum mathematical models, such as the logistic equation and the Fisher–Kolmogorov equation, can describe the global characteristics observed in commonly used cell biology assays, such as proliferation and scratch assays. However, these continuum models do not account for single-cell-level mechanics observed in high-throughput experiments. Mathematical modelling frameworks that represent individual cells, often called agent-based models, can successfully describe key single-cell-level features of these assays but are computationally infeasible when dealing with large populations. In this work, we propose an agent-based model with crowding effects that is computationally efficient and matches the logistic and Fisher–Kolmogorov equations in parameter regimes relevant to proliferation and scratch assays, respectively. This stochastic agent-based model allows multiple agents to be contained within compartments on an underlying lattice, thereby reducing the computational storage compared to existing agent-based models that allow one agent per site only. We propose a systematic method to determine a suitable compartment size. Implementing this compartment-based model with this compartment size provides a balance between computational storage, local resolution of agent behaviour and agreement with classical continuum descriptions.

1. Introduction

Cell-level processes, including proliferation, death and migration, drive tissue-level processes during regeneration, development and repair [1–3]. Traditionally, mathematical models of development and repair account for such tissue-level processes by modelling the cell population density with ordinary differential equations (ODEs) [4–7] and partial differential equations (PDEs) [8–10]. These continuum descriptions can be parametrized to predict the cell population density growth profile in commonly used cell biology assays, such as *proliferation assays* [5–7,11,12] and *scratch assays* [8–10,13,14]. In a proliferation assay (figure 1), cells are seeded uniformly on a two-dimensional substrate. Due to this initial placement of cells (figure 1*a*,*c*), there are no macroscopic spatial gradients in cell population density at the beginning of the experiment. As the experiment proceeds (figure 1*b*,*d*), individual cells undergo movement and proliferation events, with the net result being a gradual increase in the density of the monolayer towards some maximum carrying capacity density. A common mathematical model to describe these proliferation assays is the logistic equation [4–7],

$$\frac{\mathrm{d}C(t)}{\mathrm{d}t} = \lambda C(t)\left(1 - \frac{C(t)}{K}\right), \tag{1.1}$$

where $C(t)$ is the cell population density at time $t \geq 0$, $\lambda > 0$ is the cell proliferation rate and $K > 0$ is the carrying capacity. In a scratch assay (figure 2), a uniform

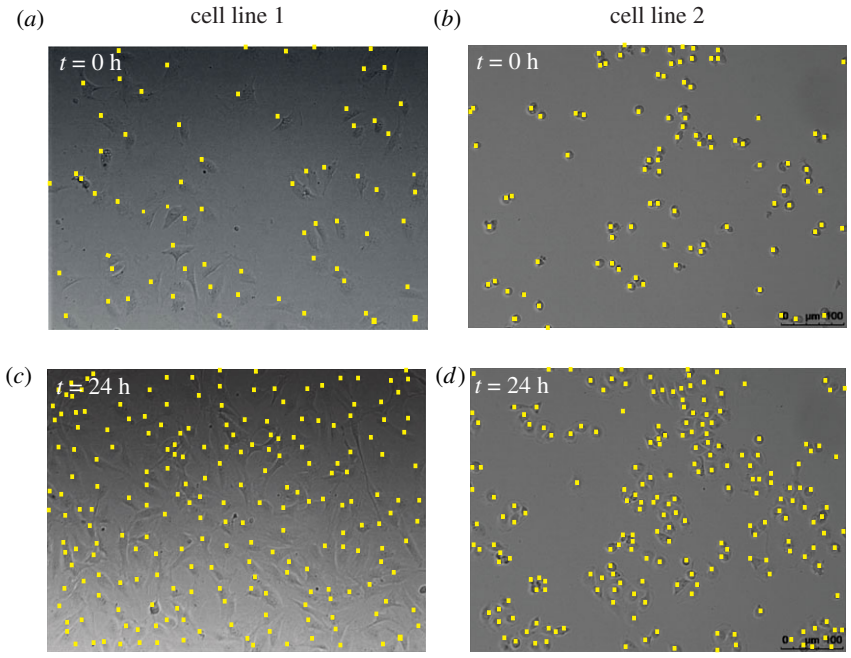

Figure 1. Images of cell proliferation assays. Images in (*a*,*c*) show a cell proliferation assay with epithelial 3T3 fibroblast cells (cell line 1) [15], while images in (*b*,*d*) show a cell proliferation assay with mesenchymal MDA-MB-231 breast cancer cells (cell line 2) [16]. The location of cells is highlighted with a yellow marker. The size of images is 640 µm × 480 µm. All images reproduced with permission from [6]. (Online version in colour.)

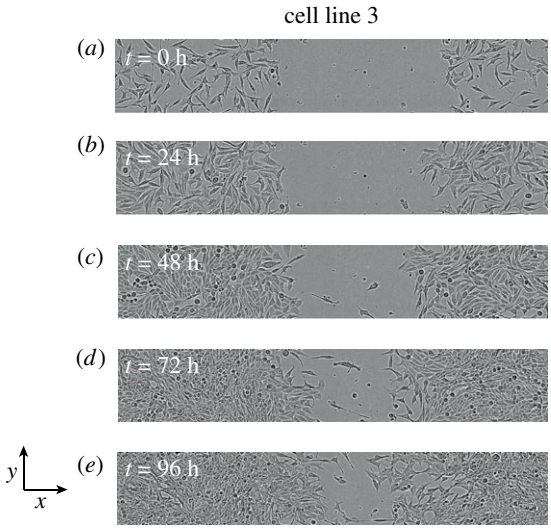

Figure 2. Images of a scratch assay. Images in (*a*–*e*) show the progression of a scratch assay performed with epithelial C4-2B prostate cancer cells (cell line 3) [17]. The size of images is 1800 µm × 300 µm. The fronts of cells move towards the centre of the initially vacant region as time progresses. All images reproduced with permission from [14].

scratch is made in a cell monolayer and observations are made of the time-dependent movement of the resulting fronts of cells. As the initial scratch creates macroscopic spatial variation in the monolayer, the cell density evolves in both time and space. A common mathematical model to describe these scratch assays is the Fisher–Kolmogorov equation [8,9,13,14,18,19],

$$\frac{\partial C(x,y,t)}{\partial t} = \lambda C(x,y,t)\left(1-\frac{C(x,y,t)}{K}\right) + D\nabla^2 C(x,y,t), \tag{1.2}$$

where $C(x, y, t)$ is the cell density at time t and position (x, y), and $D > 0$ is the diffusivity of the cell density.

While equations (1.1) and (1.2) can match the evolution of cell population densities in experiments [8], these models focus exclusively on the characteristics of the *global* cell population. However, recent technology [9,14,20,21] has made it possible to perform these assays in a high-throughput fashion, allowing hundreds of identically prepared proliferation or scratch assays to be simultaneously performed, as well as to collect single-cell-level data from these assays. With the availability of single-cell-level data, including real-time tracking of cells [20,21], different types of mathematical models that focus on cell-tracking and single-cell-level mechanics are desirable. This modelling approach is especially important since cell-tracking technology is not always accurate, especially in experiments where the cell density is high [22,23]. A convenient way to model individual cells is in a stochastic mathematical framework; these models are often called *stochastic agent-based models* [5,7,19,24,25], whereby cells are modelled as *agents*, often constrained to an underlying lattice.

A common spatial discretization for stochastic agent-based models [5,7,19,24,25] involves choosing the lattice spacing to be equal to a typical cell diameter. This spatial discretization is a natural choice when agent-based models include crowding effects, often referred to as an *exclusion process*, since lattice sites are limited to binary occupancy of a single agent. However, employing these models with this level of local resolution can be computationally infeasible for a large number of agents [26], whereas the computational storage of the analagous continuum model description is independent of the number of agents. This demand of large computational storage motivates us to consider other spatial discretizations. For instance, one could instead choose the lattice spacing to be m times the size of a typical cell diameter, where $m > 1$ is an integer, allowing multiple agents to be accommodated within each lattice *compartment*. An immediate consequence of choosing $m > 1$ is a reduction in computational storage, since the computational memory requirement reduces from $\mathcal{O}(\mathcal{N})$, where $\mathcal{N}$ is the number of agents, to

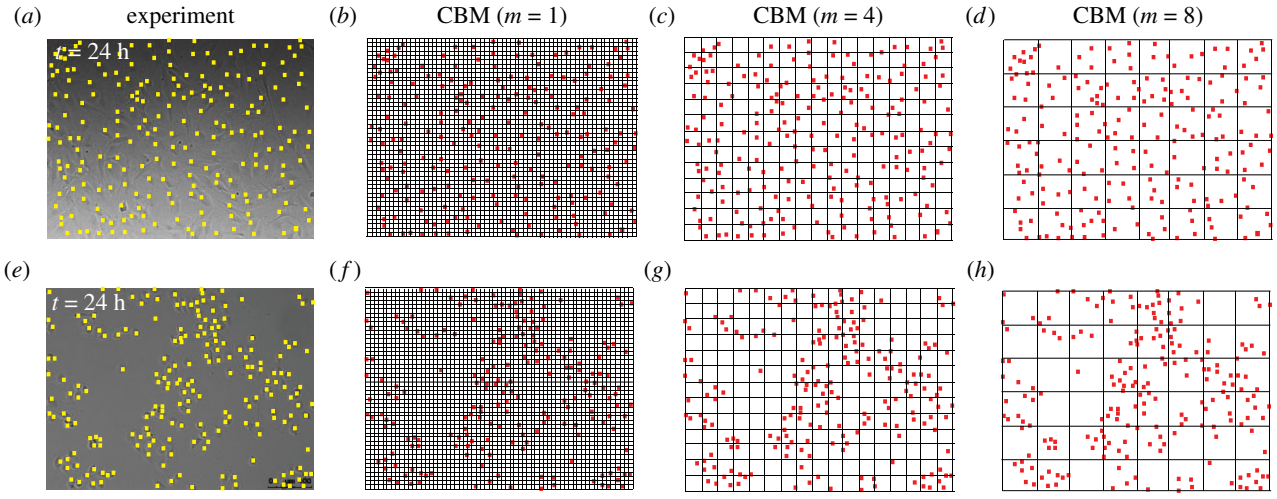

Figure 3. Choices of compartment size in the CBM. Images of proliferation assays using cell lines 1 and 2, from figure 1*c*,*d*, are shown in (*a*,*e*), respectively. Images in (*b*)–(*d*) show various discretizations of the arrangement of cells in (*a*) with $m = 1$, 4, 8, respectively. Images in (*f*–*h*) show various discretizations of the arrangement of cells in (*e*) with $m = 1$, 4, 8, respectively. (Online version in colour.)

$\mathcal{O}(\mathcal{N}/m^2)$, where $\mathcal{N}/m^2$ is the number of compartments. However, this reduction in computational storage comes at the cost of losing local agent resolution, so the key question is: how do we choose this lattice compartment size to capture local agent dynamics while still being computationally efficient?

In this work, we propose a modification to previous descriptions of stochastic agent-based models on lattices (e.g. [5,7,19]) to: (i) allow for computationally efficient simulations, (ii) capture local agent dynamics, and (iii) provide reliable agreement of the average agent density to traditional continuum model descriptions. This *compartment-based model* (CBM) discretizes space using lattice compartments with $m > 1$ (figure 3). The CBM also encodes additional biologically inspired features, such as crowding effects, whereby potential movement and proliferation events cannot occur if the target compartment is fully occupied with agents. Inclusion of crowding distinguishes the CBM from other agent-based models that describe reaction–diffusion processes [27–34] and provides additional biological realism, since many experimental observations confirm that crowding effects are very important in proliferation assays and scratch assays [1,3,5,6,11].

We compare the CBM with ODE and PDE descriptions, since traditional continuum models provide well-understood explicit solutions to key features of experiments, such as the temporal evolution of the agent density [5–8,11,12,19,24,25]. We do this by examining the *continuum limit* of the CBM, which describes the salient features of the CBM in the limit when the number of lattice sites is large [5,7,11,19,24,25]. We explore how the predicted average density of agents changes for different compartment sizes. In particular, with larger m, the CBM allows us to retain the use of traditional continuum descriptions when cell clustering is either absent (figure 1*a*,*b*) or present (figure 1*c*,*d*). Previous examination of stochastic agent-based models [5,7,19] reveals that when the proliferation-to-motility rate ratio is not sufficiently small, clustering develops and the resulting agent density profile no longer matches the solution of the continuum limit when $m = 1$ (equations (1.1) and (1.2)). However, the CBM avoids this disagreement by using a sufficiently large compartment size. We show that, for a suitable choice of m, the average agent density determined by the CBM agrees well with the solution of the continuum limit and provides a balance between computational storage and local agent information.

2. Model

We begin by presenting the CBM on a two-dimensional square lattice (figure 3) to describe simulations of both proliferation and scratch assays. Additional results (electronic supplementary material) demonstrate how the CBM generalizes to three-dimensional lattices that are relevant for three-dimensional assays.

2.1. Lattice discretization

As we focus on employing the CBM to describe two-dimensional assays (figure 3), we consider ways to discretize an $I\hat{\Delta} \times J\hat{\Delta}$ rectangle with a square lattice. Here, $\hat{\Delta}$ is a typical cell diameter (20–25 µm [6]), implying that there can be at most $\mathcal{N} = IJ$ agents on the lattice under square packing. To compare different cell lines with different cell diameters, we non-dimensionalize the lattice to have unit length spacing by setting $\hat{\Delta} = L\Delta$, where $\Delta = 1$ and L is the cell diameter [5,6,25]. We focus on non-dimensional lattices and represent the location of the top right corner of each site in Cartesian co-ordinates as $(x_i, y_j) = (i\Delta, j\Delta)$, where $i = 1, \ldots, I$ and $j = 1, \ldots, J$.

The CBM discretizes this underlying lattice into *compartments*. These compartments, of size $m\Delta \times m\Delta$, can contain up to m^2 agents. To ensure that the dimensions of the original $I\hat{\Delta} \times J\hat{\Delta}$ rectangle remain consistent under this discretization, we have $X = I/m$ compartments in the x-direction and $Y = J/m$ compartments in the y-direction. We index each $m \times m$ compartment with co-ordinates $(x_i, y_j) = (i\ m\Delta, j\ m\Delta)$, where $i = 1, \ldots, X$ and $j = 1, \ldots, Y$. While the total number of compartments in the CBM is $\mathcal{N}/m^2$, the maximum number of agents on the lattice stays at $\mathcal{N}$.

The CBM is an extension of previous agent-based models with crowding [5,7,19], in which each compartment can be occupied by at most one agent ($m = 1$). Here, the distinguishing feature of the CBM is the fact that each compartment can be

occupied by more than one agent when $m > 1$ and the key question is how we choose m to reduce computational storage while retaining sufficient local resolution. In figure 3, snapshots of proliferation assays are used to motivate the choice of m. As previously mentioned, the CBM with $m = 1$ (figure 3*b*,*f*) demands significant computational memory for large numbers of agents. Contrastingly, employing the CBM with $m > 1$ (figure 3*c*,*d*,*g*,*h*) reduces the computational storage. Both of these advantages, along with a systematic method of determining an appropriate compartment size, will be discussed in §3.

2.2. Compartment-based model

Since crowding effects are important in cell biology assays [5,7,9,19,25], the CBM is an exclusion process, as both movement and proliferation processes may only take place if the target compartment (i.e. either the same or an adjacent compartment of the agent undergoing these processes) has sufficient space to accommodate potential motility and movement events. For lattice-based models, such as the CBM, the excluded volume is the volume occupied by agents; however, this equivalence is not true for lattice-free agent-based models [35,36]. At any time, a randomly chosen isolated agent has a transition rate r_m per unit time of moving (either within the same compartment or to an adjacent compartment), a proliferation rate r_p per unit time of giving rise to another agent (placed either in the same or an adjacent compartment), and a death rate r_d per unit time (agent is removed). We assume that an agent is equally likely to be found at any particular location within a particular compartment; this is also known as a *well-mixed* assumption. The probability of an isolated agent attempting to move or proliferate to an adjacent compartment, rather than remain within the same compartment, is $1/m$. This probability can be interpreted as the number of configurations, for an agent placed inside a well-mixed $m \times m$ compartment, that result in the agent moving or proliferating into an adjacent compartment, $4m$, divided by the total number of configurations, $4m^2$. The probability that there is sufficient space available in the compartment selected for the agent to move or proliferate into is $1 - N/m^2$, where N is the number of agents in this compartment. We implement reflecting conditions along all boundaries of the lattice, which models zero net flux of cells into or out of the domain [9,21,37]. The initial placement of agents is discussed further in §§3.1 and 3.2. Using the Gillespie algorithm [38], we simulate the evolution of agents as a function of time and space using algorithm 1.

To quantify data from the CBM, we introduce appropriate notation. To describe a proliferation assay, we define $Q_m(t)$ as the total number of agents on the lattice discretized with a compartment size m at time t and from a single realization of the CBM. When comparing data from the CBM with the continuum limit description for a proliferation assay, we average data from the CBM using

$$\langle C_m(t) \rangle = \frac{1}{P\mathcal{N}} \sum_{p=1}^{P} Q_{m,p}(t), \tag{2.1}$$

where $Q_{m,p}(t)$ is the pth identically prepared realization of $Q_m(t)$ and P is the total number of identically prepared realizations. To describe a scratch assay, we define $Q_m(x_i, y_j, t)$ as the number of agents in each *compartment* of size m located at co-ordinates (x_i, y_j), at time t, from a single realization of the CBM. Motivated by the scratch assays in figure 2, we examine spatially dependent initial conditions that are approximately uniform in the y-direction [9,21,37,39]. To compare data from the CBM with the continuum limit description for a scratch assay with y-independent initial conditions, we average data in the y-direction alone using

$$\langle C_m(x, t) \rangle = \frac{1}{PY} \sum_{j=1}^{Y} \sum_{p=1}^{P} Q_{m,p}(x_i, y_j, t), \tag{2.2}$$

where $Q_{m,p}(x_i, y_j, t)$ denotes the number of agents in a compartment at position (x_i, y_j) in the pth identically prepared realization.

2.3. Continuum limit

An aim of this work is to formulate and implement the CBM so that the averaged data from this stochastic model are consistent with commonly used traditional continuum descriptions. Following [24,25,28], we examine the limit when the number of sites is large. In this limit, we can arrive at mathematical descriptions of the time-dependent average density by constructing approximate conservation statements and taking appropriate limits [24,25,28]. Furthermore, by assuming that the occupancy status of lattice sites is independent (normally referred to as the *mean-field approximation* [5,7,11,19,24,25]), the continuum limit of the CBM with $m = 1$ [24,25] is the two-dimensional analogue of the Fisher–Kolmogorov equation (equation (1.2)) on the domain $[1, I] \times [1, J]$, where $\lambda = r_p - r_d$, $K = 1 - r_d/r_p$ and $D = r_m\Delta^2/4$. For the CBM, we require that equation (1.2) be modified for $m > 1$; further details of these modifications appear in §3.

In the previous examination of continuum limits of stochastic agent-based models with crowding, such as the CBM with $m = 1$ [5,25], agreement between the solution of equations (1.1) and (1.2) and the averaged agent density from the stochastic model requires $r_p/r_m \ll 1$ (figure 4*a*–*d*). This agreement occurs because the mean-field approximation is valid in this parameter regime [5,7,19]. In §3, we will show that, with a suitable choice of m, agreement between the solution of the continuum limit and the CBM average agent density is excellent, even when r_p/r_m is not sufficiently small and clustering is present (figure 4*e*–*h*).

3. Results and discussion

It now remains to show how one should choose m. Since the CBM only keeps track of the occupancy of compartments, rather than individual agents' locations, the computational storage decreases as m increases. However, this comes at the cost of losing local agent resolution. Consequently, it is important to determine the *minimum* compartment size for which the average agent density of the CBM reasonably matches the solution of the continuum limit.

3.1. Simulating cell proliferation assays using the compartment-based model

We begin by employing the CBM in a setting that is appropriate for modelling a cell proliferation assay. Here, we focus on $I \times I$ lattices (i.e. $I = J$), so that $\mathcal{N} = I^2$. The proliferation assay begins with uniformly seeded agents, with no macroscopic gradients in agent density (figure 4*a*,*e*). In the context of the CBM, each site is initially populated uniformly at random, with some user-specified probability. Because of these translationally invariant initial conditions, the net flux of agents entering and leaving each compartment due to migration is zero and $\nabla^2 C = 0$ [9,21,37]. Consequently, $C(x, y, t)$ simplifies

Algorithm 1. Pseudo-code for the CBM.

Create an $I \times J$ lattice with some user-specified placement of agents; the total number of lattice sites is $\mathcal{N} = IJ$;
Divide the lattice into square compartments each with maximum capacity m^2;
Set $t = 0$;
while $t < t_{\text{end}}$ and $Q_m(t) < \mathcal{N}$ **do**
    Randomly choose an agent and determine the compartment it is contained within;
    Calculate propensity function $a(t) = (r_m + r_p + r_d)Q_m(t)$;
    Calculate the following random variables, uniformly distributed on $[0, 1]$: $\gamma_1, \gamma_2, \gamma_3, \gamma_4$;
    Calculate time step $\tau = -(\log_e \gamma_1)/a(t)$;
    $t = t + \tau$;
    $Q_m(t) = Q_m(t - \tau)$;
    Calculate $R = a(t)\gamma_2$;
    if $R \leq r_m Q_m(t)$ **then**
        Choose adjacent compartment with equal probability $1/4$;
        Calculate adjacent compartment population N_a;
        if $\gamma_3 < 1/m$ and $\gamma_4 < 1 - N_a/m^2$ **then**
            Move agent to chosen adjacent compartment;
        else
            Nothing happens;
    else if $R \in (r_m Q_m(t), (r_m + r_p)Q_m(t)]$ **then**
        if $\gamma_3 < 1/m$ **then**
            Choose adjacent compartment with equal probability $1/4$;
            Calculate adjacent compartment population N_a;
            if $\gamma_4 < 1 - N_a/m^2$ **then**
                Add an agent to chosen adjacent compartment;
                $Q_m(t) = Q_m(t) + 1$;
            else
                Nothing happens;
        else
            Calculate current compartment population N_c;
            if $\gamma_4 < 1 - N_c/m^2$ **then**
                Add an agent to current compartment;
                $Q_m(t) = Q_m(t) + 1$;
            else
                Nothing happens;
    else
        Remove agent;
        $Q_m(t) = Q_m(t) - 1$;

to a function of time only, $C(t)$, and equation (1.2) simplifies to equation (1.1), which can be written as

$$\left.\begin{aligned} \frac{\mathrm{d}C(T)}{\mathrm{d}T} &= C(T)\left(1 - \frac{C(T)}{K}\right), \\ \text{with solution } C(T) &= \frac{KC(0)\mathrm{e}^T}{K + C(0)(\mathrm{e}^T - 1)}, \end{aligned}\right\} \tag{3.1}$$

where $T = \lambda t$ and $C(0)$ is the initial agent density. Previous examination of stochastic models with $m = 1$ and $r_p/r_m \ll 1$ [5,7,13,19] reveals that the averaged model data agree well with the solution of the continuum limit, equation (3.1). Under these conditions, pairwise correlations between the occupancy status of lattice sites are negligible. From [5,7,13,19], we note that pairwise correlations are a *local* effect and need only be considered for small distances between agents.

To quantify how far sites must be separated before the correlation in occupancy is negligible, we examine the *correlation function*, $F(s, T)$ [5], using the CBM with $m = 1$. The correlation function is

$$F(s, T) = \frac{Q_s^{(2)}(T)\mathcal{N}^2}{\chi_s^{(2)} Q_1(T)^2}. \tag{3.2}$$

Here, $Q_s^{(2)}(T)$ is the number of pairs of agents separated on the underlying $m = 1$ lattice by the Euclidean distance s at time T; $\chi_s^{(2)}$ is the number of distinct lattice site pairs separated by a distance s. By denoting the discrete two-dimensional

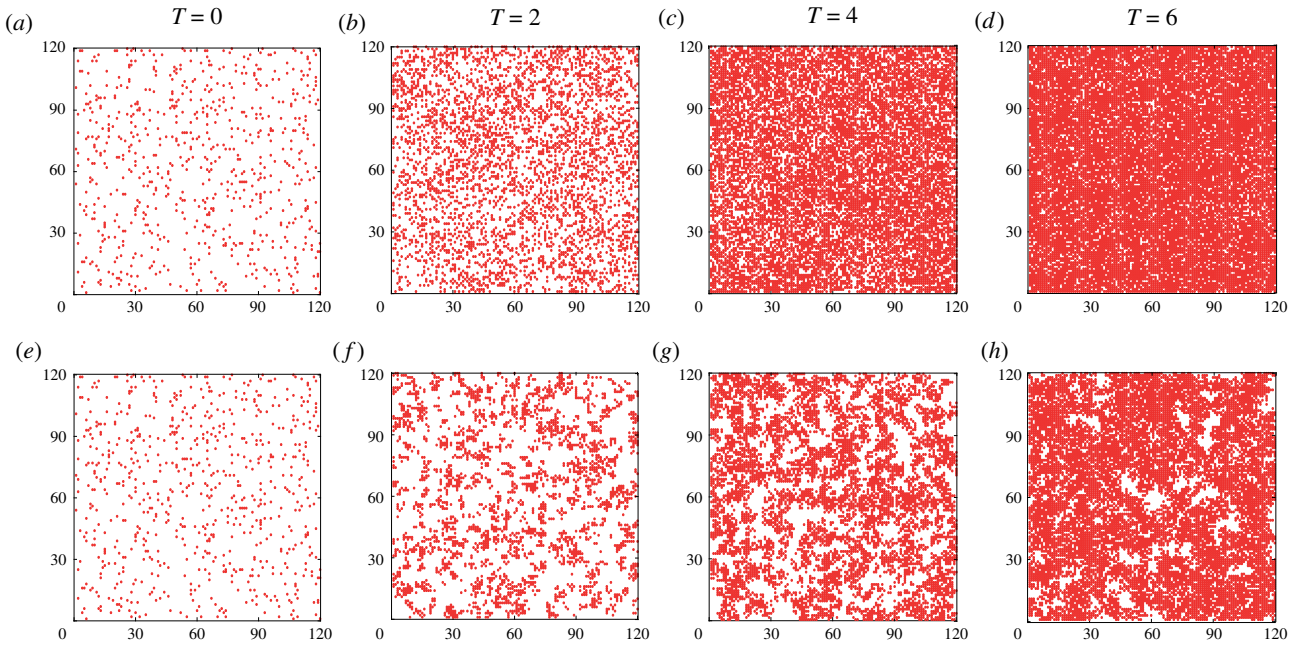

Figure 4. Simulations of two cell proliferation assays using the CBM with $m = 1$. The first simulation, shown in (*a–d*) with $r_m = 1$ and $r_p = 0.01$, results in the absence of clusters. The second simulation, shown in (*e–h*) with $r_m = 1$ and $r_p = 1$, results in clear cluster formation. In both simulations, each site of the corresponding 120×120 lattice is initially populated uniformly at random with probability 0.05. To compare simulations with different proliferation rates, we show results on the non-dimensional timescale $T = \lambda t = (r_p - r_d)t$, where $r_d = 0.1r_p$. (Online version in colour.)

Euclidean distance s as $\sqrt{\ell_1^2 + \ell_2^2}$, where $\ell_1 = 1, \ldots, I$ and $\ell_2 = 0, \ldots, \ell_1$ to prevent double-counting, we express $\chi_s^{(2)}$ as

$$\chi_s^{(2)} = \chi^{(2)}_{\sqrt{\ell_1^2+\ell_2^2}} = 2(I - \ell_1)(I - \ell_2)(2 - \delta_{\ell_1\ell_2} - \delta_{\ell_20}), \tag{3.3}$$

where δ_{ij} is the Kronecker delta. To simplify notation, we will refer to the set of discrete Euclidean distances separated by $\sqrt{\ell_1^2 + \ell_2^2}$ as $\{s_k\}$, $k \geq 1$.

If all sites are uncorrelated, $F = 1$, which is implicitly assumed in deriving the continuum limit descriptions in §2.3 [5,7,19]. To make an appropriate choice of m, we wish to determine the *threshold correlation radius*, $s_k^*(T)$, beyond which pairwise correlations are sufficiently negligible:

$$s_k^*(T) = \min_k \left\{ F(s_k, T) \middle| |F(s_k, T) - 1| < \epsilon \right\}, \tag{3.4}$$

for some user-specified tolerance $\epsilon > 0$. Furthermore, we define the *maximal correlation radius* as

$$\sigma_k^* = \max_T \langle s_k^*(T) \rangle. \tag{3.5}$$

Here, σ_k^* is implicitly a function of r_m, r_p, r_d and $C(0)$, and $\langle s_k^*(T) \rangle$ is the average of $s_k^*(T)$ over many realizations of the CBM with $m = 1$.

The maximal correlation radius, σ_k^*, is straightforward to compute, with the advantage that it relies only on quantities that are available during a typical simulation of the CBM when $m = 1$, for any r_m, r_p, r_d and $C(0)$. We now show how to determine a suitable compartment size m from σ_k^*. There are many ways to choose the *minimum* compartment size, denoted as m^*, from σ_k^*, provided that m^* is a monotonic non-decreasing function in σ_k^* and that $m^* = 1$ when the mean-field approximation is satisfied up to the tolerance ϵ. We will consider the function

$$m^* = \lceil 2\sigma_{k-1}^* \rceil, \tag{3.6}$$

since all significant pairwise correlations are contained within a compartment *diameter* of at least $2\sigma_{k-1}^*$. Therefore, any choice of $m \geq m^*$ ensures that the mean-field approximation is satisfied up to the tolerance ϵ. We note that if the mean-field approximation is satisfied up to the tolerance ϵ for all time, then $\sigma_k^* = 1$, i.e. $k = 1$. From equation (3.6) and defining $\sigma_0^* = 1/2$, we have that $m^* = 1$ is the minimal compartment size when the mean-field approximation always holds up to tolerance ϵ.

By definition, the choice of ϵ will influence how large the maximal correlation radius σ_k^* becomes. However, there is good agreement between the average agent density of the CBM with $m = 1$ and the solution of the continuum limit when $r_p/r_m \ll 1$ [5,7,19], and we should choose ϵ in such a fashion that $\sigma_k^* \approx 1$ in this parameter regime. Previous results in [5,7], as well as the electronic supplementary material of this work, show that when $F < 1.5$, there is excellent agreement between the CBM ($m = 1$) and the solution of the continuum limit, implying that $\epsilon < 0.5$ is sufficiently small. Indeed, as shown in figure 5*a*, employing the CBM in this parameter regime with larger compartment sizes ($m = 4$, 6) does not significantly affect the agreement between $\langle C_m(T) \rangle$ and $C(T)$.

Knowing that $s_k^*(T)$ is constructed to provide an agreement between the average agent density of the CBM and the solution of the continuum limit where clustering is absent, we now examine parameter regimes where agent clustering is present. As is evident in figure 4*e–h*, clusters of agents are visually distinct when $r_p/r_m = 1$, providing a suitable parameter regime to test how robust the CBM is. Results in figure 5*b* confirm that the agreement between $\langle C_m(T) \rangle$ and $C(T)$ improves as the compartment size m increases. Additionally, we note that the threshold correlation distance $s_k^*(T)$ predicts that $\sigma_k^* \approx \sqrt{5}$ (yellow curves, figures 5*c*,*d*), implying, from equation (3.6), that $m^* \approx \lceil 2 \cdot 2 \rceil = 4$ is the minimum compartment size to sufficiently contain pairwise correlations in this parameter regime. Therefore, we do not expect that the average agent density from the CBM would agree with the solution of the continuum limit in this parameter regime for $m = 1$. Nevertheless, a compartment size m larger than m^* (say, $m = 6$, green curve in figure 5*b*) is sufficient in obtaining reasonable agreement.

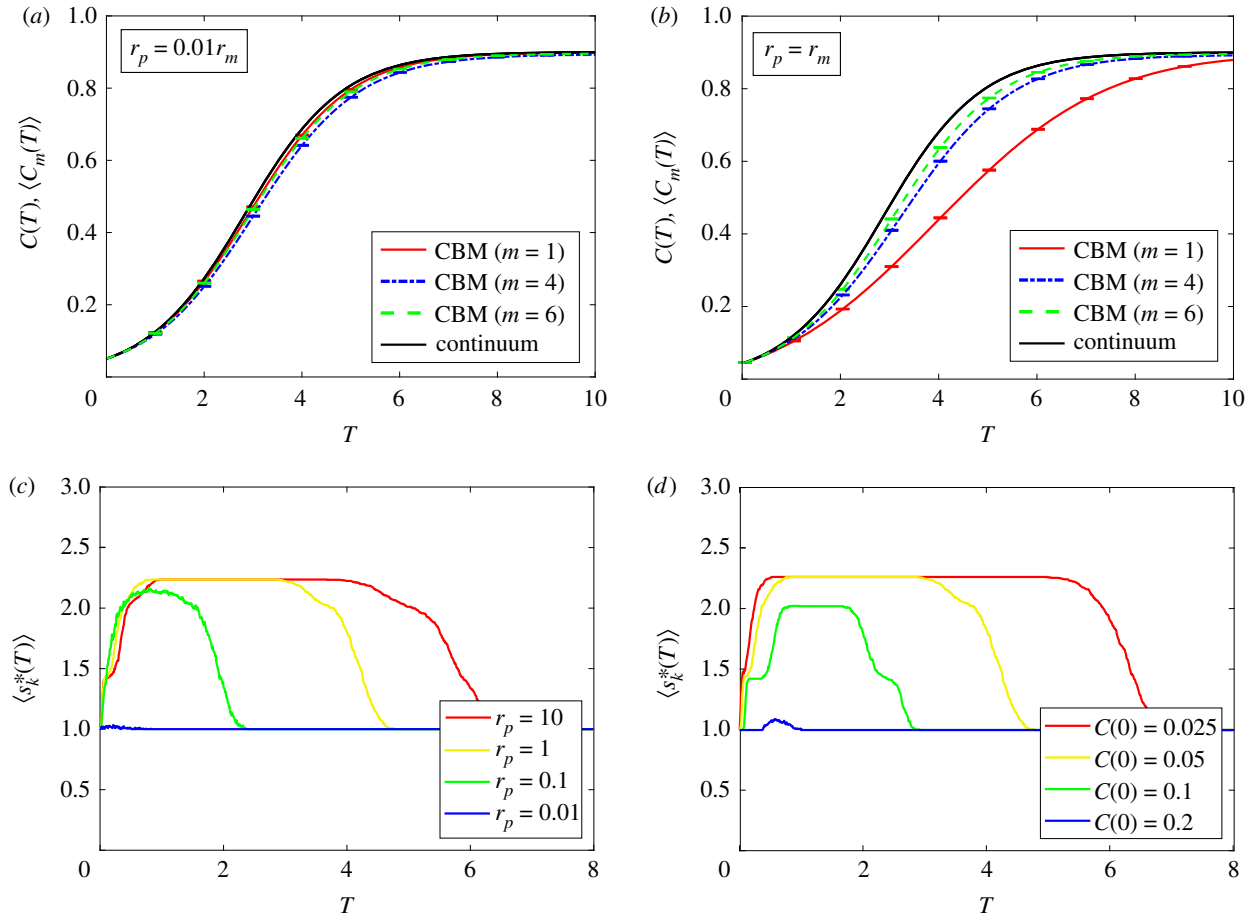

Figure 5. Simulations of a proliferation assay with the CBM. The CBM uses a 120×120 lattice, $r_m = 1$ and $r_d = 0.1 r_p$, while $\langle s_k^*(T)\rangle$, defined in equation (3.4), uses the tolerance $\epsilon = 0.3$. In all simulations, we use the same initial conditions as in figure 4. Averaged density data in (*a*,*b*) are constructed using 100 identically prepared realizations of the CBM. Results are shown for the CBM with $m = 1$, $m = 4$ and $m = 6$, and the continuum limit is given by equation (3.1). In (*a*), $r_p = 0.01$; in (*b*), $r_p = 1$. In both (*a*) and (*b*), the maximum standard error (electronic supplementary material) is less than 0.002. (*c*) Comparisons of $\langle s_k^*(T)\rangle$ for various choices of r_p. (*d*) Comparisons of $\langle s_k^*(T)\rangle$ for various choices of $C(0)$ with $r_p = 1$. (Online version in colour.)

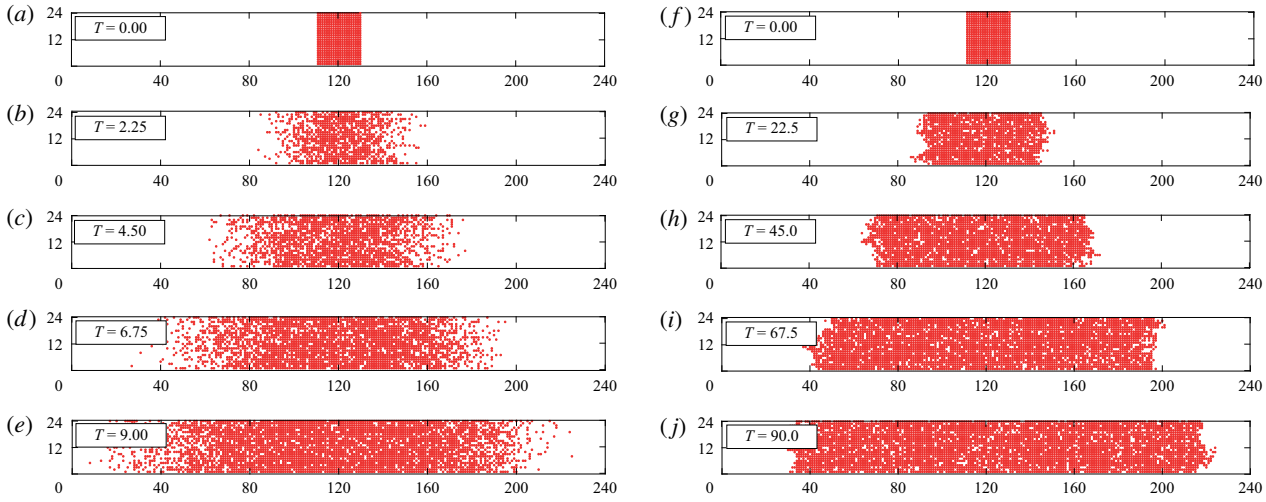

Figure 6. Simulations of two scratch assays using the CBM with $m = 1$. The first simulation, shown in (*a*–*e*) with $r_m = 1$ and $r_p = 0.01$, results in diffuse fronts and the absence of clusters. The second simulation, shown in (*f*–*j*) with $r_m = 1$ and $r_p = 1$, results in clear cluster formation. Both simulations use a 24×240 lattice that is initially fully occupied with agents in the region $110 < x \leq 130$. In all simulations, $r_d = 0.1 r_p$. (Online version in colour.)

Finally, we examine how $\langle s_k^*(T)\rangle$ varies with r_p/r_m and $C(0)$. Without loss of generality, we set $r_m = 1$ and examine the influence of r_p and $C(0)$ on $\langle s_k^*(T)\rangle$. As shown in figure 5*c*, the maximum value of $\langle s_k^*(T)\rangle$, which is σ_k^*, decreases as r_p decreases. This is to be expected; a small r_p/r_m corresponds to parameter regimes where the average agent density of the CBM with $m = 1$ matches the solution of the continuum limit. Furthermore, this same phenomenon happens when $C(0)$ is *increased* (figure 5*d*). Therefore, in parameter regimes where $C(0)$ is small, or when r_p/r_m is sufficiently large, $m^* > 1$ and thus disagreement is expected. Consequently, choosing a compartment size $m > m^*$ in the CBM reduces computational storage requirements, provides better agreement with the solution of the continuum limit when agent clustering is present and retains local agent behaviour.

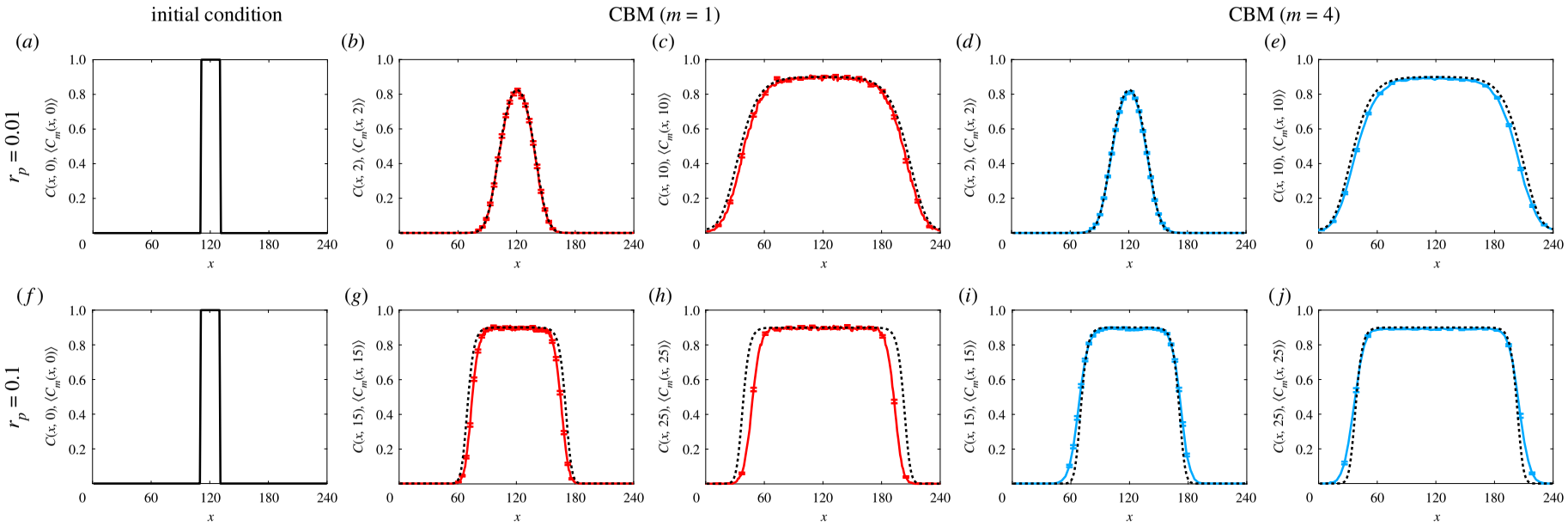

Figure 7. Simulations of a scratch assay with the CBM. Averaged density data from the CBM (solid colour curves) from 100 identically prepared simulations are compared with the solution of the continuum limit, equation (3.7) (dashed black curves), for two different scratch assay scenarios. Results are shown for the CBM with compartment size (*b*,*c*,*g*,*h*) $m = 1$ and (*d*,*e*,*i*,*j*) $m = 4$. In all simulations, we use a 24×240 lattice, with initial conditions shown in (*a*,*f*), $r_d = 0.1\ r_p$, and $r_m = 1/m$ to keep $\hat{D}$ invariant for varying m. Top row: $r_p = 0.01$, with data given at (*b*,*d*) $T = 2$, (*c*,*e*) $T = 10$. Bottom row: $r_p = 0.1$, with data given at (*g*,*i*) $T = 15$, (*h*,*j*) $T = 25$. The maximum standard error (electronic supplementary material) is less than 0.012. (Online version in colour.)

3.2. Simulating scratch assays using the compartment-based model

Now having demonstrated that, for a suitable m and ϵ, the average agent density of the CBM agrees with the solution of the continuum limit for cell proliferation assays, we examine how the CBM can be used to describe scratch assays by employing spatially varying initial conditions (figure 6). We consider simulations of scratch assays where clustering is absent (see cell line 1 in figures 1 and 6*a–e*) and simulations of scratch assays where clustering is present (cell line 2 in figure 1 and 6*f –j*). To apply the CBM, we must first consider how the diffusion term in equation (1.2), $D\nabla^2 C$, changes when varying m. Previous examination of the continuum limit of diffusion-only compartment-based models [28,29] reveals that the jump rates between adjacent compartments scale with $1/m^2$, for $m > 1$. However, the models proposed in [28,29] assume that an isolated agent will always leave its compartment, rather than having non-zero probability to remain within its compartment. Since agents in the CBM attempt to move out of a particular compartment with probability $1/m$, we divide the scaled diffusivity proposed in [28,29], $m^2 D$, by m. Therefore, the diffusivity D of the CBM continuum limit with $m = 1$ becomes mD for the CBM continuum limit with $m > 1$, and the continuum limit description of CBM simulations of scratch assays can be written as

$$\frac{\partial C(x,T)}{\partial T} = C(x,T)\left(1 - \frac{C(x,T)}{K}\right) + \hat{D}\frac{\partial^2 C(x,T)}{\partial x^2}, \qquad (3.7)$$

where $\hat{D} = mD/\lambda$. This continuum description is valid when the initial conditions are independent of y [39], such as in figures 2, 6 and 7.

Unlike in §3.1, it is less obvious how to determine m^* when describing scratch assays. This is because the threshold correlation radius (s_k^* from §3.1) will depend on both T and x, due to the spatially dependent initial conditions. While there are many ways one could determine m^* from $s_k^*(x, T)$, for simplicity, we choose the same m^* determined from equation (3.6) in §3.1. When $r_p/r_m \ll 1$ (e.g. $r_p = 0.01$, figure 7*a–e*), $m^* = 1$ and the average agent density of the CBM, $\langle C_m(x, T)\rangle$, agrees well with the solution of equation (3.7) for different compartment sizes and different times. However, for larger proliferation rates (e.g. $r_p = 0.1$, figure 7*f –j*), the fronts in the CBM become more disperse as m increases. While the CBM with $m = 1$ predicts slower-moving fronts than the solution of the continuum limit (figure 7*g*,*h*), the CBM with an intermediate compartment size ($m = m^* = 4$) agrees well with the solution of the continuum limit on the timescale shown in figure 7*i*,*j*. For larger compartment sizes, the fronts in the CBM are overly disperse and the agreement with the solution of the continuum limit diminishes. These benefits continue to hold for CBM simulations of scratch assays with different initial cell densities (electronic supplementary material). Nevertheless, the average agent density of the CBM, $\langle C_m(x, T)\rangle$, can produce qualitatively similar results to the solution of the associated continuum limit for a suitable compartment size, while requiring less computational storage than previously described stochastic agent-based models.

4. Conclusion

In this work, we propose a computationally efficient and accurate agent-based model that can be used to simulate two-dimensional cell biology assays. This CBM stems from the previous examination of cell proliferation assays, where an initially uniform distribution of biological cells move and proliferate to give rise to a monolayer of cells whose density increases with time. We also apply the CBM to scratch assays, which are prepared by scratching a monolayer of cells and observing the movement of the resulting fronts of cells. The CBM faithfully describes the behaviour of individual cells in these cell biology assays while requiring less computational overhead than other lattice models [5,7,19] when modelling large numbers of cells. Furthermore, in parameter regimes that are prone to cell clustering, the average cell density determined by these previous models does not always agree with their continuum description.

We show that the CBM is more computationally efficient than previously proposed exclusion process models on lattices through the discretization of the underlying lattice into compartments containing multiple agents. These mesoscale compartments in the CBM provide a balance between traditional continuum models and other agent-based on-lattice models that demand significant computational storage for large numbers of cells. Furthermore, when compartments larger than a threshold size are employed, the CBM agrees well with the continuum description for all physically relevant parameter regimes, including when cell clustering is present. We find that this threshold compartment size is the lattice distance beyond which pairwise correlations of agents are negligible and can be computed directly from the lattice-based model, rather than relying on continuum approximations. Furthermore, this threshold distance is a function of the cell proliferation-to-motility ratio, as well as the initial cell density. We see good agreement between the average agent density of the CBM and the continuum description both in translationally invariant environments (cell proliferation assays) and with spatially dependent initial conditions (scratch assays).

Further extensions to the description of the CBM can be made when comparing to other cell biology experiments. For example, three-dimensional gel proliferation assays describe the proliferation of agents in a three-dimensional material. By considering a three-dimensional setting (see electronic supplementary material), we can describe these gel proliferation assays using the CBM. Other kinds of assays observe the chemotactic movement of cells. By biasing the agent movement between compartments (see electronic supplementary material), we can describe these chemotactic assays using the CBM. However, the description of the CBM can be further extended to represent additional phenomena present in other biological experiments, including (but not limited to) lattice-free models with crowding, modelling multiple cell types with different proliferation and motility rates, modelling multiple cell types of different sizes and describing Allee-type dynamics within a single cell type.

Data accessibility. All Matlab codes used to generate results shown in figures 3–7 can be found at: https://github.com/nfadai/Fadai2019.

Authors' contributions. N.T.F. created the algorithm code, produced figures 3–7 and carried out the analysis of the results; M.J.S. conceived of the study, designed the study, supervised the study and helped draft figures 3–7; R.E.B. participated in the design of the study. N.T.F. wrote the paper, on which all other authors commented and made revisions. All authors gave final approval for publication.

Competing interests. We declare we have no competing interests.

Funding. This work is supported by the Australian Research Council (grant no. DP170100474). M.J.S. appreciates support from the University of Canterbury Erskine Fellowship. R.E.B. is a Royal Society Wolfson Research Merit Award holder, would like to thank the Leverhulme

Trust for a Research Fellowship and also acknowledges the BBSRC for funding via grant no. BB/R000816/1.

Acknowledgements. We thank the two anonymous referees for their helpful comments.

References

1. Abercrombie M. 1979 Contact inhibition and malignancy. *Nature* **281**, 259–262. (doi:10.1038/281259a0)
2. Barrandon Y, Green H. 1987 Cell migration is essential for sustained growth of keratinocyte colonies: the roles of transforming growth factor-α and epidermal growth factor. *Cell* **50**, 1131–1137. (doi:10.1016/0092-8674(87)90179-6)
3. Ward M, McCann C, DeWulf M, Wu JY, Rao Y. 2003 Distinguishing between directional guidance and motility regulation in neuronal migration. *J. Neurosci.* **23**, 5170–5177. (doi:10.1523/JNEUROSCI.23-12-05170.2003)
4. Murray JD. 2003 *Mathematical biology I: an introduction*. Berlin, Germany: Springer-Verlag.
5. Baker RE, Simpson MJ. 2010 Correcting mean-field approximations for birth-death-movement processes. *Phys. Rev. E* **82**, 041905. (doi:10.1103/physreve.82.041905)
6. Simpson MJ, Binder BJ, Haridas P, Wood BK, Treloar KK, McElwain DLS, Baker RE. 2013 Experimental and modelling investigation of monolayer development with clustering. *Bull. Math. Biol.* **75**, 871–889. (doi:10.1007/s11538-013-9839-0)
7. Markham DC, Simpson MJ, Baker RE. 2013 Simplified method for including spatial correlations in mean-field approximations. *Phys. Rev. E* **87**, 062702. (doi:10.1103/PhysRevE.87.062702)
8. Maini PK, McElwain DS, Leavesley DI. 2004 Traveling wave model to interpret a wound-healing cell migration assay for human peritoneal mesothelial cells. *Tissue Eng.* **10**, 475–482. (doi:10.1089/107632704323061834)
9. Jin W, Shah ET, Penington CJ, McCue SW, Chopin LK, Simpson MJ. 2016 Reproducibility of scratch assays is affected by the initial degree of confluence: experiments, modelling and model selection. *J. Theor. Biol.* **390**, 136–145. (doi:10.1016/j.jtbi.2015.10.040)
10. Ponce-Bobadilla V, Arévalo J, Sarró E, Byrne H, Maini P, Carraro T, Meseguer A, Alarcon T. 2019 *In vitro* cell migration quantification method for scratch assays. *J. R. Soc. Interface* **16**, 20180709. (doi:10.1098/rsif.2018.0709)
11. Cai AQ, Landman KA, Hughes BD. 2007 Multi-scale modeling of a wound-healing cell migration assay. *J. Theor. Biol.* **245**, 576–594. (doi:10.1016/j.jtbi.2006.10.024)
12. Tremel A, Cai A, Tirtaatmadja N, Hughes BD, Stevens GW, Landman KA, O'Connor AJ. 2009 Cell migration and proliferation during monolayer formation and wound healing. *Chem. Eng. Sci.* **64**, 247–253. (doi:10.1016/j.ces.2008.10.008)
13. Markham DC, Simpson MJ, Maini PK, Gaffney EA, Baker RE. 2014 Comparing methods for modelling spreading cell fronts. *J. Theor. Biol.* **353**, 95–103. (doi:10.1016/j.jtbi.2014.02.023)
14. Jin W. 2017 Investigating the reproducibility of *in vitro* cell biology assays using mathematical models. PhD thesis, Queensland University of Technology. See http://eprints.qut.edu.au/109790.
15. Todaro GJ, Green H. 1963 Quantitative studies of the growth of mouse embryo cells in culture and their development into established lines. *J. Cell Biol.* **17**, 299–313. (doi:10.1083/jcb.17.2.299)
16. Cailleau R, Young R, Olive M, Reeves Jr W. 1974 Breast tumor cell lines from pleural effusions. *J. Natl Cancer Inst.* **53**, 661–674. (doi:10.1093/jnci/53.3.661)
17. Thalmann GN, Anezinis PE, Chang S-M, Zhau HE, Kim EE, Hopwood VL, Pathak S, von Eschenbach AC, Chung LW. 1994 Androgen-independent cancer progression and bone metastasis in the LNCaP model of human prostate cancer. *Cancer Res.* **54**, 2577–2581.
18. Fisher RA. 1937 The wave of advance of advantageous genes. *Ann. Eugen.* **7**, 355–369. (doi:10.1111/j.1469-1809.1937.tb02153.x)
19. Simpson MJ, Baker RE. 2011 Corrected mean-field models for spatially dependent advection-diffusion-reaction phenomena. *Phys. Rev. E* **83**, 051922. (doi:10.1103/physreve.83.051922)
20. Huth J, Buchholz M, Kraus JM, Mølhave K, Gradinaru C, Wichert Gv, Gress TM, Neumann H, Kestler HA. 2011 TimeLapseAnalyzer: multi-target analysis for live-cell imaging and time-lapse microscopy. *Comput. Methods Programs Biomed.* **104**, 227–234. (doi:10.1016/j.cmpb.2011.06.002)
21. Johnston ST, Shah ET, Chopin LK, McElwain DLS, Simpson MJ. 2015 Estimating cell diffusivity and cell proliferation rate by interpreting IncuCyte ZOOM assay data using the Fisher-Kolmogorov model. *BMC Syst. Biol.* **9**, 38. (doi:10.1186/s12918-015-0182-y)
22. Doxzen K, Vedula SRK, Leong MC, Hirata H, Gov NS, Kabla AJ, Ladoux B, Lim CT. 2013 Guidance of collective cell migration by substrate geometry. *Integr. Biol.* **5**, 1026–1035. (doi:10.1039/c3ib40054a)
23. Simpson MJ, Binder BJ, Haridas P, Wood BK, Treloar KK, McElwain DLS, Baker RE. 2013 Quantifying the roles of cell motility and cell proliferation in a circular barrier assay. *J. R. Soc. Interface* **10**, 20130007. (doi:10.1098/rsif.2013.0007)
24. Simpson MJ, Landman KA, Hughes BD. 2009 Multi-species simple exclusion processes. *Physica A* **388**, 399–406. (doi:10.1016/j.physa.2008.10.038)
25. Simpson MJ, Landman KA, Hughes BD. 2010 Cell invasion with proliferation mechanisms motivated by time-lapse data. *Physica A* **389**, 3779–3790. (doi:10.1016/j.physa.2010.05.020)
26. Fahse L, Wissel C, Grimm V. 1998 Reconciling classical and individual-based approaches in theoretical population ecology: a protocol for extracting population parameters from individual-based models. *Am. Nat.* **152**, 838–852. (doi:10.1086/286212)
27. Anguige K, Schmeiser C. 2009 A one-dimensional model of cell diffusion and aggregation, incorporating volume filling and cell-to-cell adhesion. *J. Math. Biol.* **58**, 395–427. (doi:10.1007/s00285-008-0197-8)
28. Taylor PR, Yates CA, Simpson MJ, Baker RE. 2015 Reconciling transport models across scales: the role of volume exclusion. *Phys. Rev. E* **92**, 040701. (doi:10.1103/PhysRevE.92.040701)
29. Taylor PR, Baker RE, Simpson MJ, Yates CA. 2016 Coupling volume-excluding compartment-based models of diffusion at different scales: Voronoi and pseudo-compartment approaches. *J. R. Soc. Interface* **13**, 20160336. (doi:10.1098/rsif.2016.0336)
30. Engblom S, Ferm L, Hellander A, Lötstedt P. 2009 Simulation of stochastic reaction-diffusion processes on unstructured meshes. *SIAM J. Sci. Comput.* **31**, 1774–1797. (doi:10.1137/080721388)
31. Erban R, Chapman SJ. 2009 Stochastic modelling of reaction–diffusion processes: algorithms for bimolecular reactions. *Phys. Biol.* **6**, 046001. (doi:10.1088/1478-3975/6/4/046001)
32. Drawert B, Lawson MJ, Petzold L, Khammash M. 2010 The diffusive finite state projection algorithm for efficient simulation of the stochastic reaction-diffusion master equation. *J. Chem. Phys.* **132**, 074101. (doi:10.1063/1.3310809)
33. Black AJ, McKane AJ. 2012 Stochastic formulation of ecological models and their applications. *Trends Ecol. Evol.* **27**, 337–345. (doi:10.1016/j.tree.2012.01.014)
34. Smith S, Cianci C, Grima R. 2016 Analytical approximations for spatial stochastic gene expression in single cells and tissues. *J. R. Soc. Interface* **13**, 20151051. (doi:10.1098/rsif.2015.1051)
35. Smith S, Cianci C, Grima R. 2017 Macromolecular crowding directs the motion of small molecules inside cells. *J. R. Soc. Interface* **14**, 20170047. (doi:10.1098/rsif.2017.0047)
36. Cianci C, Smith S, Grima R. 2017 Capturing Brownian dynamics with an on-lattice model of hard-sphere diffusion. *Phys. Rev. E* **95**, 052118. (doi:10.1103/PhysRevE.95.052118)
37. Simpson MJ, Landman KA, Hughes BD. 2009 Pathlines in exclusion processes. *Phys. Rev. E* **79**, 031920. (doi:10.1103/PhysRevE.79.031920)
38. Gillespie DT. 1977 Exact stochastic simulation of coupled chemical reactions. *J. Phys. Chem.* **81**, 2340–2361. (doi:10.1021/j100540a008)
39. Simpson MJ. 2009 Depth-averaging errors in reactive transport modeling. *Water Resour. Res.* **45**, W02505. (doi:10.1029/2008WR007356)